J Mater Sci: Mater Med (2013) 24:1799–1807
DOI 10.1007/s10856-013-4923-4

Nano-composite scaffolds for bone tissue engineering containing silver nanoparticles: preparation, characterization and biological properties

Eleonora Marsich · Francesca Bellomo · Gianluca Turco · Andrea Travan · Ivan Donati · Sergio Paoletti

Received: 17 December 2012 / Accepted: 24 March 2013 / Published online: 4 April 2013

Abstract In this study nano-composite scaffolds to be used as bone grafts have been endowed with antibacterial properties owing to the presence of silver nanoparticles. The alginate/hydroxyapatite composite scaffolds were prepared by internal gelation followed by a freeze-drying procedure to obtain a porous structure. The nanoparticles were prepared in presence of a lactose modified-chitosan and this colloidal solution was adsorbed on the scaffolds by exploiting electrostatic interactions. The adsorption and release of the silver from the composite scaffold was measured by ICP-AES and spectrofluorimetry measurements. Micro-computed tomography analysis of the scaffolds showed a homogeneous porous structure with average pore sizes of 341.5 μm and porosity of 80 %. In vitro biological tests (MTS and killing kinetics assays) demonstrated that silver does not affect the ability of the scaffolds to promote osteoblasts proliferation and that at the same time it exerts a strong bactericidal effect against both Gram+ and Gram− bacterial strains. Overall, the combined results indicate that these biocompatible antimicrobial scaffolds possess ideal characteristics for tissue engineering applications.

E. Marsich · G. Turco
Department of Medical, Surgical and Health Sciences, University of Trieste, Piazza dell'Ospitale 1, 34129 Trieste, Italy

E. Marsich (✉) · A. Travan · I. Donati · S. Paoletti
Department of Life Sciences, University of Trieste, Via Giorgieri 5, 34127 Trieste, Italy
e-mail: emarsich@units.it

F. Bellomo
Department of Life Sciences, University of Trieste, Via Giorgieri 1, 34127 Trieste, Italy

1 Introduction

The presence of a foreign material, such as a synthetic biomaterial, in the body of the implant recipient represents a potential site for microbial attachment [1, 2]. Reducing bacterial adhesion is important since microorganism surface attachment is the first critical step in the development of implant-associated infections. To overcome the limitations of antibiotic treatments for the prevention of periprosthetic infections, particular attention is devoted to the use of alternative antimicrobial agents such as copper, zinc and silver [3–6]. Silver is a broad spectrum antibacterial agent and it is used in both ionic and metallic forms and it is particularly employed as nanoparticles in colloidal solutions [7]. The antimicrobial activity has been related mainly to its oxidized form (Ag^{+}) and it causes disruption of bacterial cell membranes, inhibition of enzymatic activities, ATP production within ion transport processes and DNA replication [8]. The reactivity of silver is further enhanced when it is used in nanosized particles, which possess an enormous surface-to-volume ratio and higher reactivity than the bulk element. Several studies reported the antimicrobial effects of silver nanoparticles (AgNPs) for a range of different bacterial strains of clinical relevance [9]. Hence, silver has become the most used antimicrobial nanomaterial for medical treatment and health care in recent years [10]. As far as orthopaedic and dental fields are concerned, silver-based compounds have been used to functionalize implantable permanent devices for the localised delivery of broad-spectrum bactericidal molecules to treat and prevent implant-based infections. Acrylic and ceramic bone cements loaded with Ag^{+} in different chemical forms and with various physical–chemical approaches showed high effectiveness against multiresistant bacteria in vitro [11–14]. Several recent studies reported the use of

Ag-based compounds to reduce bacterial and fungal infections associated with titanium implants. Tyllianakis et al. [15] proposed copolymers endowed with antimicrobial activity due to the entrapment of silver-covered titanium nanocrystals in the matrix. Das et al. [16] modified titanium surface with silver-treated titania nanotubes in order to concomitantly improve bone cell–implant interaction and antimicrobial activities. Jaiswal et al. [4] reported that AgNPs immobilized within hydrogel coatings on titanium guarantee for antibacterial activity while preserving osteoblasts' response at the implant interface. As resorbable bone fillers, antibacterial scaffolds containing chitosan and nano-hydroxyapatite were developed by preparing silver particles through a chemical reduction reaction of silver nitrate by the functional groups of chitosan [17]. Our group recently devised a strategy [18] to produce novel scaffolds based on alginate and nanohydroxyapatite (Alg/nHap) able to efficiently support the adhesion and proliferation of cells, showing at the same time structural and physical–chemical properties adequate to confer good osteoconductive and osteointegration features as resorbable bone grafts. The goal of this study is to endow these scaffolds with antibacterial properties by introducing AgNPs by means of a physisorption process at room temperature in order to maintain the scaffold micro-structural properties and its efficacy in supporting cell growth.

2 Materials and methods

2.1 Preparation of alginate and hydroxyapatite composites (Alg/nHap) scaffolds

Alginate ($F_G = 0.69$; $F_{GG} = 0.56$; MW = 130,000) was kindly provided by FMC biopolymers (Drammen, Norway). Alg/nHap composite scaffolds were prepared by mixing alginate 2 % (w/v) and nHap 3 % (w/v) in water using a calcium release method according to [18]. nHap powder was homogenously dispersed into a stirred solution of alginate in water, followed by the addition of GDL at a final concentration of 60 mM to displace calcium ions from nHap. Aliquots of the gelling solution were then cured in 24-well tissue culture plates (h = 18 mm, Ø = 16 mm, Costar, Cambridge, MA, USA) for 24 h at room temperature to allow complete gelification. The hydrogels in the tissue-culture plate were then step-wise cooled by immersion in a liquid cryostat. Ethylene Glycol in water (3:1) was used as refrigerant fluid. Temperature was decreased step-wise from 20 to −20 °C by 5 °C steps with 30 min intervals for equilibration; the samples were then freeze-dried for 24 h to obtain porous scaffolds.

2.2 Chitlac-silver nanoparticles synthesis (Chitlac-nAg)

Chitlac (lactose-modified chitosan, CAS registry number 85941-43-1) was prepared according to the procedure reported elsewhere [19] starting from a highly deacetylated chitosan [residual acetylation degree approximately 18 %, Aldrich chemical Co. (U.S.A.)]. The (viscosity average) relative molar mass of chitosan was estimated to be approximately 7×10^5. The composition of Chitlac was determined by means of ^{1}H-NMR and resulted to be glucosamine residue = 20 %; *N*-acetylglucosamine = 18 %; and 2-(lactit-1-yl)-glucosamine = 62 %. The relative molecular mass of Chitlac is $\sim 1.5 \times 10^6$.

Silver nanoparticles were obtained by reducing silver ions with ascorbic acid in Chitlac solutions according to the following procedures [20]: freeze-dried Chitlac was dissolved in deionized water to obtain solution with final concentration 2 g/l. Chitlac solution were mixed with $AgNO_3$ solution to achieve a final $AgNO_3$ concentrations of 1 mM; the ascorbic acid ($C_6H_8O_6$) solution was added at final concentration of 0.5 mM.

2.3 Preparation of scaffolds embedding Chitlac-nAg

The colloidal solution of Chitlac-nAg was sterilized by filtration through a 0.2 μm filter (Millipore). 1.5 ml of solution were added to each lyophilized scaffold Alg/nHap (average diameter of 16 mm and a thickness of 10 mm) in a 24 multiwell plate. The scaffolds were incubated overnight at room temperature and then washed extensively with deionized water to remove non adsorbed Chitlac. Scaffolds (Chitlac-nAg scaffolds) were then freeze-dried, sterilized by UV irradiation and used for the biological tests.

2.4 Chitlac-fluorescein (Chitlac-FITC) synthesis

Chitlac (200 mg) was dissolved in 67 ml of 0.5 M sodium carbonate buffer. Fluorescein-isothiocyanate (FITC, Sigma) were dissolved in 7 ml of 0.5 M sodium carbonate buffer and added drop wise to the Chitlac solution to label 1/2,000 of available amino groups. The reaction mixture was stirred overnight at room temperature, against $NaHCO_3$ 0,1 M, and against de-ionized water until the conductivity of the external solution was below 2 μS at 4 °C (Spectrapore, MWCO 12,000) for 12 h. All procedures were carried out under dark condition. The solutions were filtered trough 0, 45 μm filters and freeze dried.

2.5 Inductively coupled plasma-atomic emission spectrometry

The quantitative analysis of the silver concentration was performed by means of ICP-AES using a Spectroflame module E Optical plasma interface (OPI) instrument by SPECTRO (Germany).

The total amount of silver in the Chitlac-nAg scaffolds was measured upon treatment with aqua regia (concentrated nitric acid and concentrated hydrochloric acid—1:3). The scaffolds (cylindrical in shape with an average diameter of 16 mm and a thickness of 10 mm) were solubilised with 5 ml of aqua regia, under stirring condition for 1 h at about 100 °C, then filtered through 0.45 μm GHP acrodisc syringe filters (Pall Life Science, Ann Arbor, MI, USA) and the volume adjusted to 25 ml with deionized water. The average amount of silver in a scaffold was calculated as the mean of silver quantity in six samples.

Silver released from nAg-containing scaffolds was evaluated upon immersion in 3 ml of washing solution (NaCl 0.15 M) in agitation at room temperature; after incubation for different periods of time, supernatant from the scaffolds was diluted with water up to NaCl 0.015 M, aqua regia was added to prevent metal reduction and silver concentration quantised by ICP-AES after sample centrifugation and filtration with a membrane of Teflon 0.42 μm (Millipore-USA).

The obtained values have been compared with a calibration curve calculated with a standard solution of silver (Silver ICP/DCP-Sigma Aldrich) 10,000 μg/ml in HNO_3. The used wavelength was 328.068 nm and with detection limit of 0.02 mg/l. The coefficient of correlation was higher than 0.998.

The washing solution was changed every 24 h with the aim to maximize the stress on the structural stability of the constructs for detecting the maximum release of silver. The silver released every 24 h was then measured.

Each test was performed on seven scaffolds and the results are reported as the average of data obtained from them.

2.6 Scanning electron microscopy (SEM)

Scaffolds structure was analyzed using a Quanta250 Scanning Electron microscope (FEI, Oregon, USA). Freeze-casted samples were sectioned at various planes and directly visualized by electron microscopy after sputter-coating with an ultrathin layer of gold.

2.7 X-ray microcomputed tomography (μ-CT)

X-ray microcomputed tomography of samples was obtained by means of a cone–beam system called TOMOLAB (www.elettra.trieste.it/Labs/TOMOLAB). The device is equipped with a sealed microfocus X-ray tube, which guarantees a focal spot size of 5 μm in an energy range from 40 up to 130 kV, and a maximum current of 300 μA. As a detector, a CCD digital camera was used with a 49.9 × 33.2 mm^2 field of view and a pixel size of 12.5 × 12.5 μm^2. The samples were positioned onto the turn-table of the instrument and acquisitions were performed with the following parameters: distance source-sample (FOD), 100 mm; distance source-detector (FDD), 400 mm; magnification, 4×; binning, 2 × 2; resolution, 6.25 μm; tomographies dimensions (pixels), 1,984 × 1,024; slices dimensions (pixels), 1,984 × 1,984; number of tomographies, 1,440; number of slices, 864; (*E*) 40 kV, (*I*) 200 μA; exposure time, from 2 to 5 s. The slices reconstruction process achieved by means of commercial software (Cobra Exxim) started once the tomographic scan was completed and all the projections were transferred to the workstation. Input projections and output slices are represented by files (one file per projection and one file per slice) using arrays of 16-bit integers. Custom produced MatLab code has been used to get a proper segmentation of the slices using Otsu's [21] method and to obtain numerical values of structural features like porosity, interconnection, pore, and trabecular size by means of parallel plate model [18, 22].

2.8 Antimicrobial tests

The antibacterial activity of Chitlac-nAg scaffolds was evaluated using cultures of *Escherichia coli* (ATCC25922), *Staphylococcus epidermidis* (clinical isolate), *Staphylococcus aureus* (ATCC252922) and *Pseudomonas aeruginosa* (ATCC 27853).

Bacterial suspensions were prepared by adding 20 μl of bacteria, preserved in glycerol, to 5 ml of LB (Luria–Bertani) broth. The obtained suspensions were incubated *o/n* at 37 °C. After 24 h, 500 μl of bacterial suspension was diluted in 15 ml of broth and grown for 60–90 min at 37 °C. Bacterial concentration was measured by means of optical density (O.D.) spectrometric measurement at 600 nm. The bacterial suspension was then diluted in 30 % (v/v) LB broth in PBS (phosphate buffered saline) to obtain a final concentration of 10^5 bacteria/ml. In a 24-multiwell plate, 1 ml of bacterial suspension was added to each scaffold. The plates were incubated at 37 °C under shaking for defined times. At the end of incubation, the bacterial suspension was transferred in a 15 ml tube and the scaffolds were washed with 1 ml of PBS by vortexing for 30 s. The washing solution was then added to the bacterial suspension previously transferred into the tube. The total collected bacterial solution was serially diluted in PBS (from 10^{-1} to 10^{-6}) and plated in duplicate on LB agar. After incubation *o/n* at 37 °C the colony forming units (CFUs) were counted.

2.9 Cell culture and viability test on Chitlac-nAg scaffolds

Osteosarcoma MG-63 (ATCC® Number: CRL-1427™) human cell line was cultured in DMEM supplemented with 10 % FBS, 1 % penicillin–streptomycin/1 % L-glutamine at 37 °C and 5 % pCO_2. Saos-2 (ATCC® Number: HTB-85™) human osteosarcoma cell line was maintained in McCoy's Medium with 15 % FBS, 1 % penicillin–streptomycin/1 % L-glutamine at 37 °C and 5 % pCO_2.

For cell seeding onto scaffolds, freeze-casted scaffolds produced under sterile conditions were reswollen in 5 mM $CaCl_2$ for 10 min under agitation and immersed in complete cell culture medium for 12 h in 24-wells culture plates to ensure chemical equilibration. Approximately 4×10^4 cells, suspended in 50 µl of medium, were loaded with a micropipette over the whole upper surface of the scaffold. After 4 h, the scaffolds were placed into fresh, sterile 24-well culture plates and 1 mL of complete medium was added.

The viability and growth rate of MG63 and Saos-2 cell lines on Chitlac-nAg composites were assessed as a function of time using the MTS assay according to the protocol provided by the manufacturer (CellTiter Aqueous One Solution cell proliferation Assay kit from Promega). MTS assay was performed in quadruplicate 1, 2, 5 and 7 days from cell seeding. Briefly, after 4 h of incubation with the MTS reagent in a humidified 5 % CO_2 atmosphere, the medium was collected from the scaffolds and absorbance was measured on an ELISA plate reader at a wavelength of 490 nm. The background absorbance obtained from empty scaffolds (blank) was subtracted from the sample values.

3 Results and discussion

3.1 Antibacterial scaffolds preparation and characterization

The strategy used in this study in order to load AgNPs inside the scaffolds is based on the electrostatic interaction between the polyanion alginate and the polycation polysaccharide (1-deoxylactit-1-yl chitosan, shortly named "Chitlac") which is a soluble at neutral pH [19]. Chitlac has been previously used to prepare and stabilize metal nanoparticles in colloidal suspension (Chitlac-nAg) and to coat methacrylic thermosets [13, 20]. Freeze-dried Alg/nHap scaffolds were immersed in the polysaccharide–AgNPs colloidal solution in order to promote the grafting of the nanocomposite coating on the construct. The porous structure of the hydrophilic scaffold was expected to allow the penetration of the colloidal solution within the alginate-based structure, leading to the formation of a Chitlac-nAg coating anchored by electrostatic forces to the trabecular surface of the scaffolds.

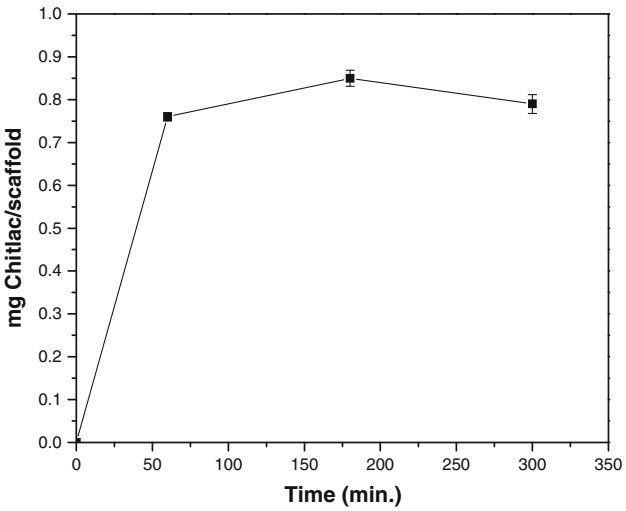

Fig. 1 Adsorption kinetic of Chitlac on Alg/Hap scaffolds. The amount of adsorbed Chitlac (in mg) is reported as a function of time

In order to quantify the adsorption of the polycation on the alginate-based constructs, the scaffolds were incubated in Chitlac labeled with a fluorescent probe (Chitlac-FITC) and, at defined intervals of time, the supernatant solution was removed and analysed by spectrofluorimetry. The amount of adsorbed Chitlac was evaluated from the difference between the initial and the residual concentration of the polysaccharide (Fig. 1).

The quantitative analysis showed that most of the polycation was adsorbed on the scaffold within 60 min and after this time there was no considerable adsorption of Chitlac; at equilibrium, an average of 0.75 ± 0.02 mg of polysaccharide was anchored on each scaffold.

After immersion of the Alg/nHap scaffolds in the polysaccharide–silver solution (Chitlac-nAg), the presence of the nanoparticles in the constructs can be pointed out by their yellow–brown color, as shown in Fig. 2a. Structural and morphological analyses of the scaffolds were performed to investigate their architectural feature, a crucial factor for a correct design of a matrix for tissue engineering. Such three-dimensional structure should possess some key requisites which include high porosity, adequate average pore size and pore size distribution to allow vascularisation and colonization by the cells; the morphology must be tailored to respond to specific application requirements as it strongly influences cell adhesion, proliferation matrix deposition and tissue organization.

The SEM characterization (Fig. 2 from b–e) pointed out that the scaffolds possess an isotropic porous interconnected homogenous structure with a pore size distribution between 150 and 450 µm.

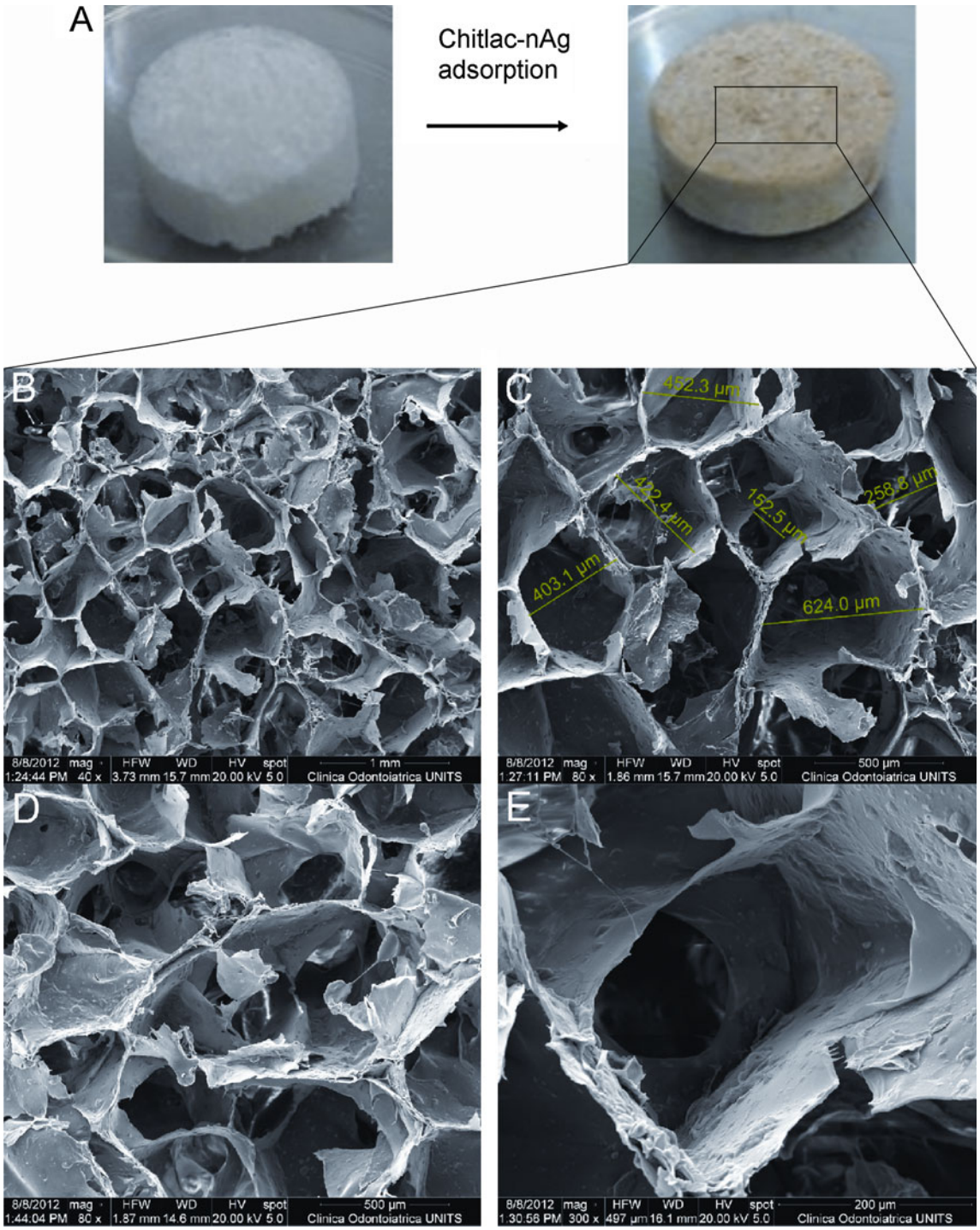

Fig. 2 **a** Macroscopic appearance of an Alg/nHap (on the *left*) and of a Chitlac-nAg scaffold (on the *right*). From **b** to **e**, SEM micrographs of Chitlac-nAg scaffolds. **b** Micrograph at magnification ×40 showing the uniform pore size distribution; **c** and **d** Micrographs at magnification ×80 showing pore dimensions and interconnectivity; **e** Micrograph at magnification ×300 showing the detail of a single pore

A three-dimensional reconstruction (Fig. 3) and a quantitative characterization of the microstructure of the scaffold concerning porosity, trabecular thickness, trabecular separation and connectivity have been performed by µ-CT analysis.

The structural parameters obtained from a data segmentation process analyzing four different 400 × 400 × 400 pixels REV with 6.25 µm/voxel resolution are reported in Table 1 and they are compared to the structural parameters of a nAg-free scaffold previously described by our group [19].

It can be observed that the parameter values of Chitlac-nAg scaffolds are slightly different from the ones previously obtained for scaffolds without silver. In particular, pore diameter and trabecular thickness are higher in nAg containing scaffolds while the porosity and connectivity density appear slightly lower. These data indicate that the physical process used to load the nanoparticles on the scaffolds (such as reswelling and Chitlac-nAg adsorption followed by freeze-drying) induce some changes in the original structure of the scaffold, which could be ascribed to the physical stress of the additional freeze-drying step.

However, all the critical morphological parameters such as interconnectivity and pore dimensions remain in a range comparable with that described as optimal for supporting cell penetration, adhesion, spreading, diffusion of nutrients and neovascularization. Previous studies reported that osteoconduction and implant osteointegration require the vascularization and growth of new bone into implant via an interconnected porosity, preferably in the 70–90 % range and 200–600 μm in size [23–25]; thus, our silver-coated scaffolds are perfectly in this range since the porosity value is about 80 % with average trabecular separation of 341 μm.

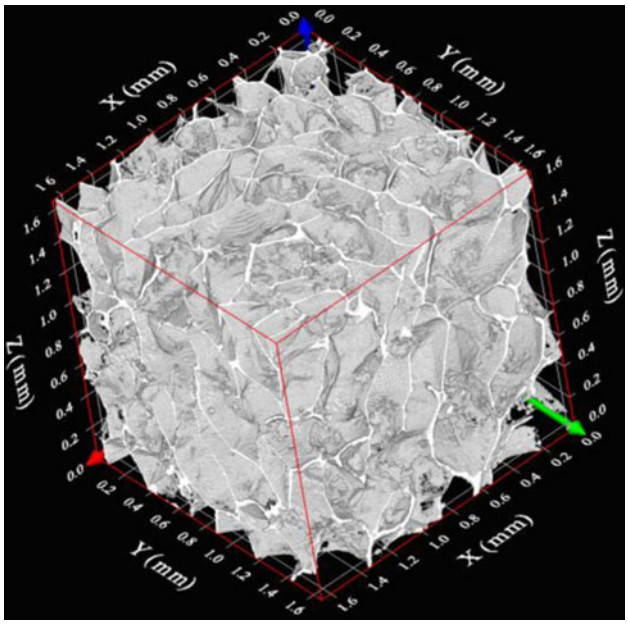

Fig. 3 Three-dimensional reconstruction of the Chitlac-nAg scaffold from μ-CT segmented data of a freeze-casted scaffold

Table 1 Quantitative parameters of the microstructure of the Chitlac-nAg samples compared with that obtained from Alg/nHap scaffolds by μ-CT analyses

Parameters	Chitlac-nAg scaffolds[a]	nAg-free scaffolds[b]
Porosity (%)	80.0 ± 2.0	88 ± 2.0
Tb.Th (μm)	61.00 ± 10.33	29.70 ± 6.25
Tb.Sp (μm)	341.50 ± 120.35	204.70 ± 6.25
BS/TV (1/mm)	56.09 ± 1.82	8.6 ± 0.3
BS/BV (1/mm)	280.45 ± 4.23	70.1 ± 1.5
Conn.D (1/mm)	2.75 ± 0.67	4.26 ± 0.89

Tb.Th trabecular thickness, *Tb.Sp* trabecular separation, *BS/TV* bone surface to total volume, *BS/BV* bone surface to bone volume, *Conn.D* connectivity density

[a] Each value is the average of four 400 × 400 × 400 pixels REV

[b] Data from Ref. [19]

In order to measure the amount of silver deposited on the Alg-nHap scaffold, ICP-AES analyses were carried out and indicated that the average quantity of silver for each scaffold was 32 ± 3 μg, corresponding approximately to 500 μg of silver for each gram of construct.

To investigate the release of silver from the scaffolds, the samples were incubated in an aqueous NaCl solution 0.15 M and the amount of silver in the supernatant was measured at different periods of time. Aqueous NaCl solution was replaced every 24 h in order to maximize the destabilisation of the alginate-based construct by an ion exchange process. The silver leached from the scaffold was evaluated every 24 h. In Fig. 4 it can be observed that the release kinetic is constant over time and that after 6 days less than 40 % of the total silver has been leached in the supernatant, corresponding to an average of 12 μg of metal for each scaffold.

3.2 In vitro biocompatibility tests

Since antimicrobial nanocomposite materials need to combine bactericidal activity with a lack of toxicity towards mammalian cells, preliminary cytotoxicity tests were carried out with human MG63 and Saos-2 osteoblast-like cells by MTS assay. The results were compared with those obtained from control scaffolds without nAg nanoparticles (Alg/nHap scaffolds). Cells were seeded at day 0

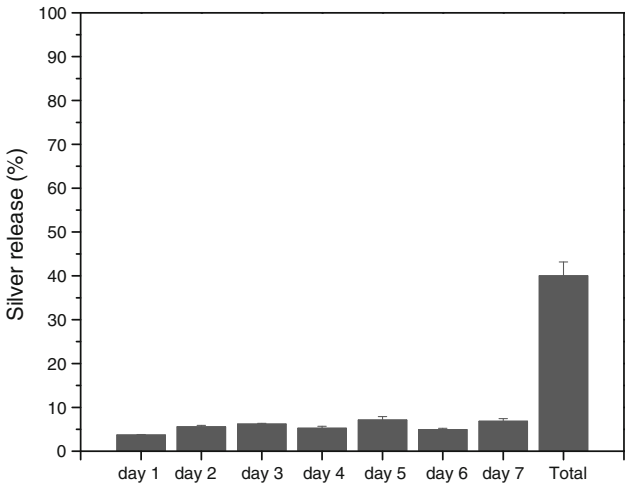

Fig. 4 Release profile of silver from Chitlac-nAg scaffolds over time. The data are expressed as percentage of silver referred to the initial amount loaded on the scaffold

on the top of the scaffolds after reswelling of the structures; the proliferation assay was performed up to days 1, 2, 5 and 7 after initial seeding. The Fig. 5 summarizes the results: the proliferation rate of cells seeded into Chitlac-nAg scaffolds is comparable and not significantly different to the one of cells grown on nAg-free constructs. This result demonstrates that nAg nanoparticles introduced into the scaffold to foster antibacterial properties, do not impair the already demonstrated adequacy [18] of constructs to sustain cell proliferation.

As already indicated by earlier studies, nanoparticles may cause adverse effects because their penetration by endocytosis into the cells and accumulation in various intracellular compartments or organelles [26]. Once the nanoparticles penetrate into the cells, they are thought to strongly interact with various protein and nucleic acid structures within these compartments, damaging or limiting various cellular functions [27–29]. The lack of toxicity observed for the nAg-scaffolds can be ascribed to the fact that the 3D system prevents the nanoparticles, embedded in the polymeric matrix, from being available for eukaryotic cellular uptake. Moreover, it is reasonable to think that although the swelling of Chitlac-nAg scaffolds in culture medium determines a release of AgNPs and/or silver ions, they are present at a concentration lower than the minimum concentration able to exert toxic effects.

3.3 Antimicrobial activity of Chitlac-nAg scaffolds

Since the focus of this study is to develop biocompatible scaffolds with antibacterial properties, we tested the antibacterial activity of Chitlac-nAg scaffolds towards four bacteria strains, both Gram+ and Gram– (*E. coli*, *P. aeruginosa*, *S. aureus* and a clinical strain of *S. epidermidis*). These strains were selected because of their occurrence in biomaterial-related infection [30, 31]. More than the 50 % of perimplant infection is caused by *S. epidermidis* [32, 33]. On the other hand *E. coli* is the typical bacterium used in laboratory to evaluate the efficacy of antimicrobial agent and antibiotics.

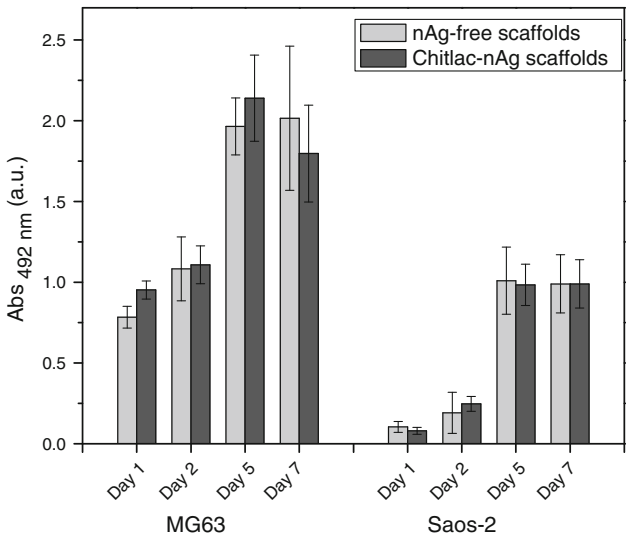

Fig. 5 Cell proliferation of MG-63 and Saos-2 cell lines as a function of time in nAg-free scaffolds and Chitlac-nAg scaffolds. MTS assay was performed at days 1, 2, 5 and 7 after initial seeding. Mean values ± SD are reported

The time killing assay was performed incubating a bacterial suspension with the scaffolds and evaluating at different times, after smearing on a solid medium, the amount of viable cells (CFU). The test was performed in shaking condition to maximize the contact between bacteria and AgNPs. The results were compared with those obtained by tests performed with Alg/nHap scaffolds without nAg and with a suspension of bacteria grown in liquid medium.

Overall, Chitlac-nAg scaffolds showed, in line with previous data [13, 20], a remarkable bactericidal effect against all four bacterial strains with a very fast killing kinetics, as reported in Fig. 6.

The Fig. 6a and b show the results obtained by *P. aeruginosa* and *E. coli*. For both strains, a slight decrease of the CFU/ml can be observed already after 30 min; after 180 min there is a drastic drop of their CFU/ml value, while Alg/nHap scaffolds do not display any antibacterial activity. After 300 min there is almost complete bacterial inactivation.

In the case of the strain of *S. aureus* (Fig. 6c) after 180 min the decrease of CFU/ml is 1.5–2 log units. After 300 min the bactericidal activity results more evident, in fact a decrease of seven orders of magnitude of their CFU/ml with respect to the controls can be observed.

In Fig. 6d the results of killing kinetics of *S. epidermidis* are reported. For this strain the bactericidal activity appears less efficient, in fact the decrease of their CFU/ml became remarkable (3–4 log units) only after 300 min of incubation with scaffolds and in this time span no complete bacteria killing is observed.

We also tested the residual antibacterial activity of Chitlac-nAg scaffolds after 10 days of immersion in a solution of NaCl. 0.15 M daily changed (Fig. 7). Although in these conditions approximately half of the total silver is released (see Fig. 4), the scaffolds showed a bactericidal activity against *S. aureus* only slightly reduced in comparison with non NaCl soaked Chitlac-nAg scaffolds. Likely, the quantity of nanoparticles loaded in the scaffolds overcomes largely the minimum concentration of metal necessary to lead to complete bacterial killing in 300 min (see Fig. 6). For this reason, although after 10 days the silver released is conspicuous, the residual nanoparticles are sufficient to guarantee a significant antibacterial activity.

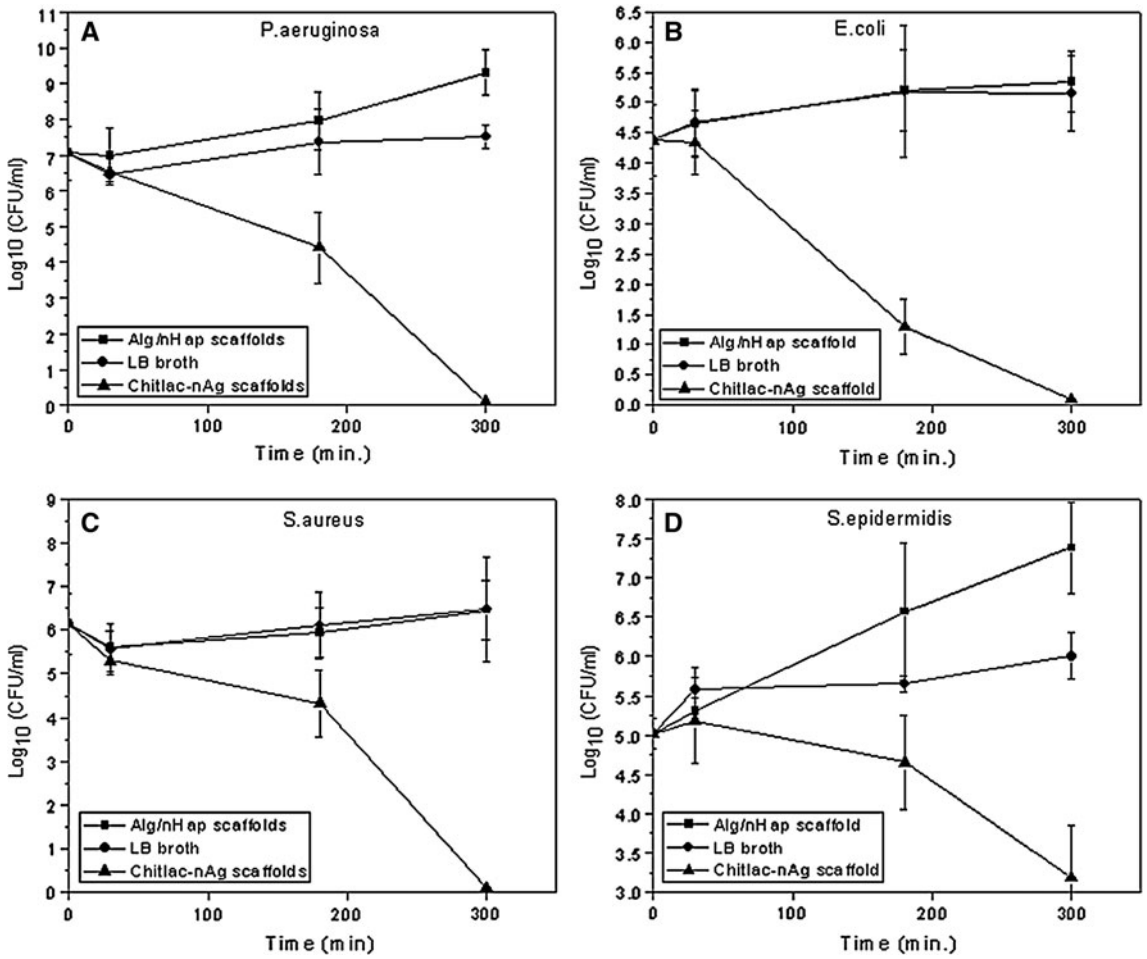

Fig. 6 Growth rate of bacteria on Chitlac-nAg scaffolds (*filled triangle*), on Alg/nHap scaffolds (*filled square*) and in LB broth (*filled circle*). **a** *P. aeruginosa*; **b** *E. coli*; **c** *S. aureus*; **d** *S. epidermidis*. Results are mean values (±SD) of five determinations

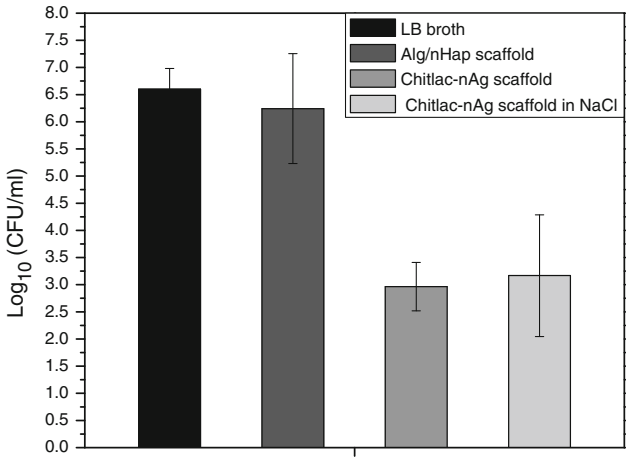

Fig. 7 Antibacterial activity against *S. aureus* of Chitlac-nAg scaffolds after their immersion in NaCl 0.15 M for 10 days. CFU/ml of bacteria grown in 300 min on NaCl treated Chitlac-nAg scaffolds (*empty square*) are compared with CFU/ml of bacteria grown in LB broth (*filled black square*), on Alg/nHap scaffolds (*filled dark grey square*) and on non-soaked Chitlac-nAg scaffolds (*filled grey square*)

4 Conclusions

Nano-composite antibacterial scaffolds have been designed by loading AgNPs with an adsorption process that does not require chemical manipulation on the scaffold. As a whole, the obtained results show that AgNPs confer to composite scaffolds good antimicrobial properties for a time-span that can be considered as adequate to confer a short-term protection from early-infections associated to the use of temporary resorbable bone implants. Considering the fact that in prosthesis implantation the surgery is always associated with antibiotic prophylaxis, the combined use of antimicrobial scaffolds and antibiotics should drastically decrease the risk of infection. An important point of strength of this paper is the concern about the effect of silver species on the surrounding cell system in implanted medical devices. In these constructs silver ions and nanoparticles release are properly controlled in order to assure antibacterial activity while preserving osteoblasts vitality.

Acknowledgments This study was supported by the EU-FP6 Project "NEWBONE" (Contract Number 026279-2). The authors would like to thank Dott. Matteo Crosera for the ICP-AES analyses.

References

1. Hetrick EM, Schoenfisch MH. Reducing implant-related infections: active release strategies. Chem Soc Rev. 2006;35(9):780–9.
2. Segawa H, Tsukayama DT, Kyle RF, Becker DA, Gustilo RB. Infection after total knee arthroplasty. A retrospective study of the treatment of eighty-one infections. J Bone Joint Surg Am. 1999;81(10):1434–45.
3. Grass G, Rensing C, Solioz M. Metallic copper as an antimicrobial surface. Appl Environ Microbiol. 2011;77(5):1541–7.
4. Jaiswal S, McHale P, Duffy B. Preparation and rapid analysis of antibacterial silver, copper and zinc doped sol–gel surfaces. Colloids Surf B. 2012;94:170–6.
5. Stankovic A, Dimitrijevic S, Uskokovic D. Influence of size scale and morphology on antibacterial properties of ZnO powders hydrothemally synthesized using different surface stabilizing agents. Colloids Surf B. 2012;102C:21–8.
6. Wilkinson LJ, White RJ, Chipman JK. Silver and nanoparticles of silver in wound dressings: a review of efficacy and safety. J Wound Care. 2011;20(11):543–9.
7. Lara HH, Garza-Trevino EN, Ixtepan-Turrent L, Singh DK. Silver nanoparticles are broad-spectrum bactericidal and virucidal compounds. J Nanobiotechnol. 2011;9:30.
8. Rai M, Yadav A, Gade A. Silver nanoparticles as a new generation of antimicrobials. Biotechnol Adv. 2001;27(1):76–83.
9. Chaloupka K, Malam Y, Seifalian AM. Nanosilver as a new generation of nanoproduct in biomedical applications. Trends Biotechnol. 2010;28(11):580–8.
10. Travan A, Marsich E, Donati I, Paoletti S. Silver nanocomposites and their biomedical applications. In: Kumar C, editor. nanocomposites. Wiley: New York; 2010. p. 81–137.
11. Alt V, Bechert T, Steinrucke P, Wagener M, Seidel P, Dingeldein E, et al. An in vitro assessment of the antibacterial properties and cytotoxicity of nanoparticulate silver bone cement. Biomaterials. 2004;25(18):4383–91.
12. Oei JD, Zhao WW, Chu L, Desilva MN, Ghimire A, Rawls HR, et al. Antimicrobial acrylic materials with in situ generated silver nanoparticles. J Biomed Mater Res B. 2011 [Epub ahead of print].
13. Travan A, Marsich E, Donati I, Benincasa M, Giazzon M, Felisari L, et al. Silver-polysaccharide nanocomposite antimicrobial coatings for methacrylic thermosets. Acta Biomater. 2011;7(1):337–46.
14. Yoshida K, Tanagawa M, Matsumoto S, Yamada T, Atsuta M. Antibacterial activity of resin composites with silver-containing materials. Eur J Oral Sci. 1999;107(4):290–6.
15. Tyllianakis M, Dalas E, Christofidou M, Kallitsis JK, Chrissanthopoulos A, Koutsoukos PG, et al. Novel composites materials from functionalized polymers and silver coated titanium oxide capable for calcium phosphate induction, control of orthopedic biofilm infections: an "in vitro" study. J Mater Sci Mater Med. 2010;21(7):2201–11.
16. Das K, Bose S, Bandyopadhyay A, Karandikar B, Gibbins BL. Surface coatings for improvement of bone cell materials and antimicrobial activities of Ti implants. J Biomed Mater Res B. 2008;87(2):455–60.
17. Saravanan S, Nethala S, Pattnaik S, Tripathi A, Moorthi A, Selvamurugan N. Preparation, characterization and antimicrobial activity of a bio-composite scaffold containing chitosan/nano-hydroxyapatite/nano-silver for bone tissue engineering. Int J Biol Macromol. 2011;49(2):188–93.
18. Turco G, Marsich E, Bellomo F, Semeraro S, Donati I, Brun F, et al. Alginate/hydroxyapatite biocomposite for bone ingrowth: a trabecular structure with high and isotropic connectivity. Biomacromolecules. 2009;10(6):1575–83.
19. Donati I, Stredanska S, Silvestrini G, Vetere A, Marcon P, Marsich E, et al. The aggregation of pig articular chondrocyte and synthesis of extracellular matrix by a lactose-modified chitosan. Biomaterials. 2005;26(9):987–98.
20. Travan A, Pelillo C, Donati I, Marsich E, Benincasa M, Scarpa T, et al. Non-cytotoxic silver nanoparticle-polysaccharide nanocomposites with antimicrobial activity. Biomacromolecules. 2009;10(6):1429–35.
21. Otsu N. A threshold selection method from gray-level histograms. IEEE Trans Syst Man Cybern. 1979;9(1):62–6.
22. Parfitt AM, Mathews CH, Villanueva AR, Kleerekoper M, Frame B, Rao DS. Relationships between surface, volume, and thickness of iliac trabecular bone in aging and in osteoporosis. Implications for the microanatomic and cellular mechanisms of bone loss. J Clin Invest. 1983;72(4):1396–409.
23. Wake MC, Patrick CW Jr, Mikos AG. Pore morphology effects on the fibrovascular tissue growth in porous polymer substrates. Cell Transplant. 1994;3(4):339–43.
24. Wang B, Chen K, Jiang S, Reincke F, Tong W, Wang D, et al. Chitosan-mediated synthesis of gold nanoparticles on patterned poly(dimethylsiloxane) surfaces. Biomacromolecules. 2006;7(4):1203–9.
25. Yang S, Leong KF, Du Z, Chua CK. The design of scaffolds for use in tissue engineering.Part I. Tissue Eng. 2001;7:679–89.
26. Lubick N. Nanosilver toxicity: ions, nanoparticles–or both? Environ Sci Technol. 2008;42(23):8617.
27. Djordjevic VB. Free radicals in cell biology. Int Rev Cytol. 2004;237:57–89.
28. Gilca M, Stoian I, Atanasiu V, Virgolici B. The oxidative hypothesis of senescence. J Postgrad Med. 2007;53(3):207–13.
29. Simon HU, Haj-Yehia A, Levi-Schaffer F. Role of reactive oxygen species (ROS) in apoptosis induction. Apoptosis. 2000;5(5):415–8.
30. Koort JK, Makinen TJ, Knuuti J, Jalava J, Aro HT. Comparative 18F-FDG PET of experimental *Staphylococcus aureus* osteomyelitis and normal bone healing. J Nucl Med. 2004;45(8):1406–11.
31. Arciola CR, Visai L, Testoni F, Arciola S, Campoccia D, Speziale P, et al. Concise survey of *Staphylococcus aureus* virulence factors that promote adhesion and damage to peri-implant tissues. Int J Artif Organs. 2011;34(9):771–80.
32. Montanaro L, Speziale P, Campoccia D, Ravaioli S, Cangini I, Pietrocola G, et al. Scenery of *Staphylococcus* implant infections in orthopedics. Future Microbiol. 2011;6(11):1329–49.
33. Uckay I, Pittet D, Vaudaux P, Sax H, Lew D, Waldvogel F. Foreign body infections due to *Staphylococcus epidermidis*. Ann Med. 2009;41(2):109–19.